

Supporting Information

Charge carrier trapping processes in lanthanide doped La-, Gd-, Y-, and LuPO₄

Tianshuai Lyu* and Pieter Dorenbos

Delft University of Technology, Faculty of Applied Sciences, Department of Radiation
Science and Technology, section Luminescence Materials, Mekelweg 15, 2629JB Delft, The
Netherlands

E-mail: T.lyu-1@tudelft.nl

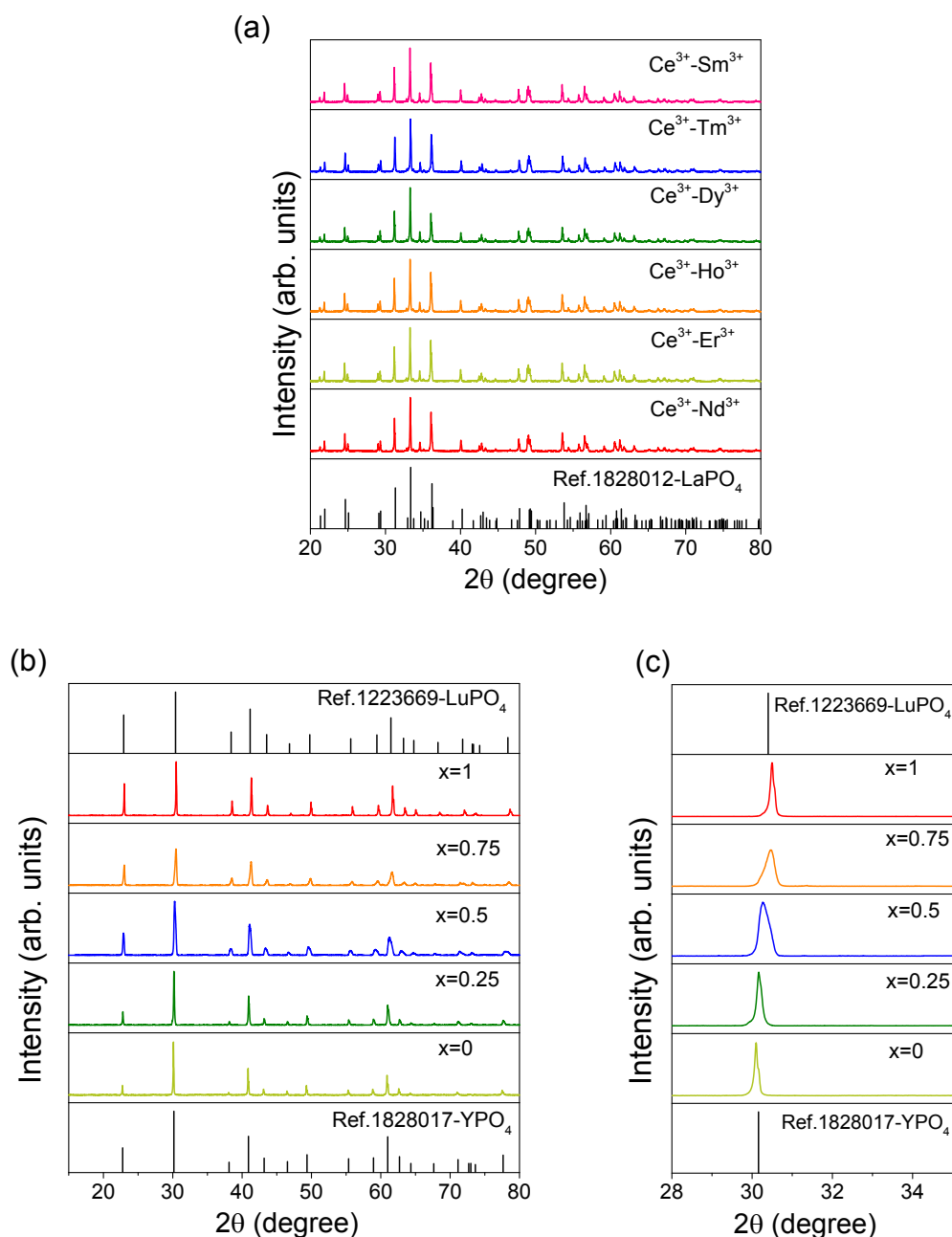


Fig. S1. XRD patterns of (a) $\text{LaPO}_4:0.005\text{Ce}^{3+},0.005\text{Ln}^{3+}$. (b) XRD patterns and (c) detailed patterns in the range from 28 to 35° for $\text{Y}_{1-x}\text{Lu}_x\text{PO}_4:0.005\text{Eu}^{3+},0.005\text{Tb}^{3+}$ solid solutions.

Fig. S1a shows the XRD patterns of $\text{LaPO}_4:0.005\text{Ce}^{3+},0.005\text{Ln}^{3+}$. All samples are of single phase and match well with the LaPO_4 reference (No. 1828012).

Fig. S1b shows the XRD patterns of $\text{Y}_{1-x}\text{Lu}_x\text{PO}_4:0.005\text{Eu}^{3+},0.005\text{Tb}^{3+}$. The XRD peaks show a slight shift towards larger 2θ angles compared to YPO_4 because lutetium ions enter into the larger yttrium sites and decrease the cell volume. With increasing x , solid solution appears since both YPO_4 and LuPO_4 have the same crystal structure (space group: $I4_1/amd O_2$).

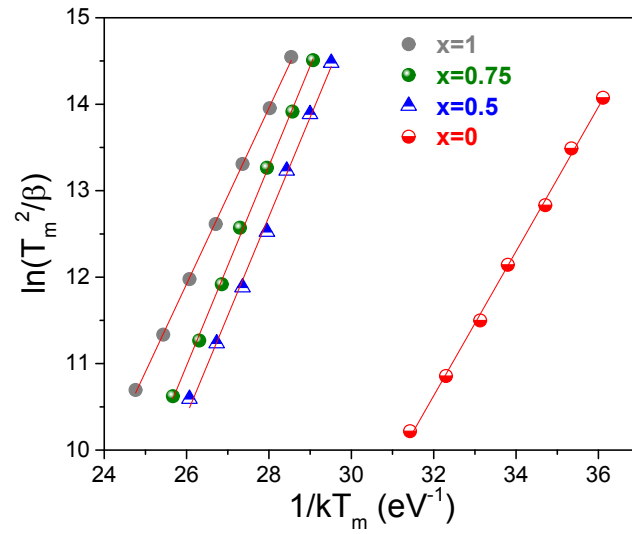


Fig. S2. Variable heating rate plots of $\text{Gd}_{1-x}\text{La}_x\text{PO}_4:0.005\text{Ce}^{3+}, 0.005\text{Ho}^{3+}$ ($x=0, 0.5, 0.75,$ and 1) solid solutions. The used heating rates were 0.08, 0.15, 0.30, 0.63, 1.25, 2.5, and 5 K/s.

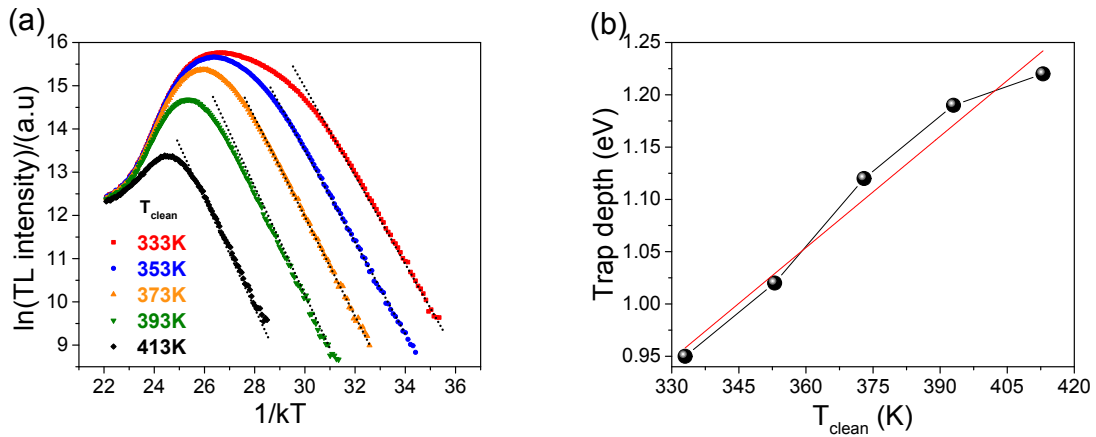


Fig. S3. (a) Initial rise analysis on all TL glow curves as a function of T_{clean} for $x=0.25$. (b) calculated trap depth. The red solid line is a linear fit through the data points.

The initial rise method was used to determine the trap depth at T_{clean} . The rising part of TL intensity ($I(T)$) can be approximated using¹⁻⁶

$$I(T) = C \times \exp\left(\frac{-E}{kT}\right) \quad (1)$$

where C is a constant. Fig. S3a shows the initial rise plots of TL glow curves for $x=0.25$ after different peak temperature T_{clean} . Straight line sections appear in the low temperature part. With increasing the T_{clean} , the trap depth derived from the slope increases from 0.95 to 1.2 eV as shown in Fig. S3b.

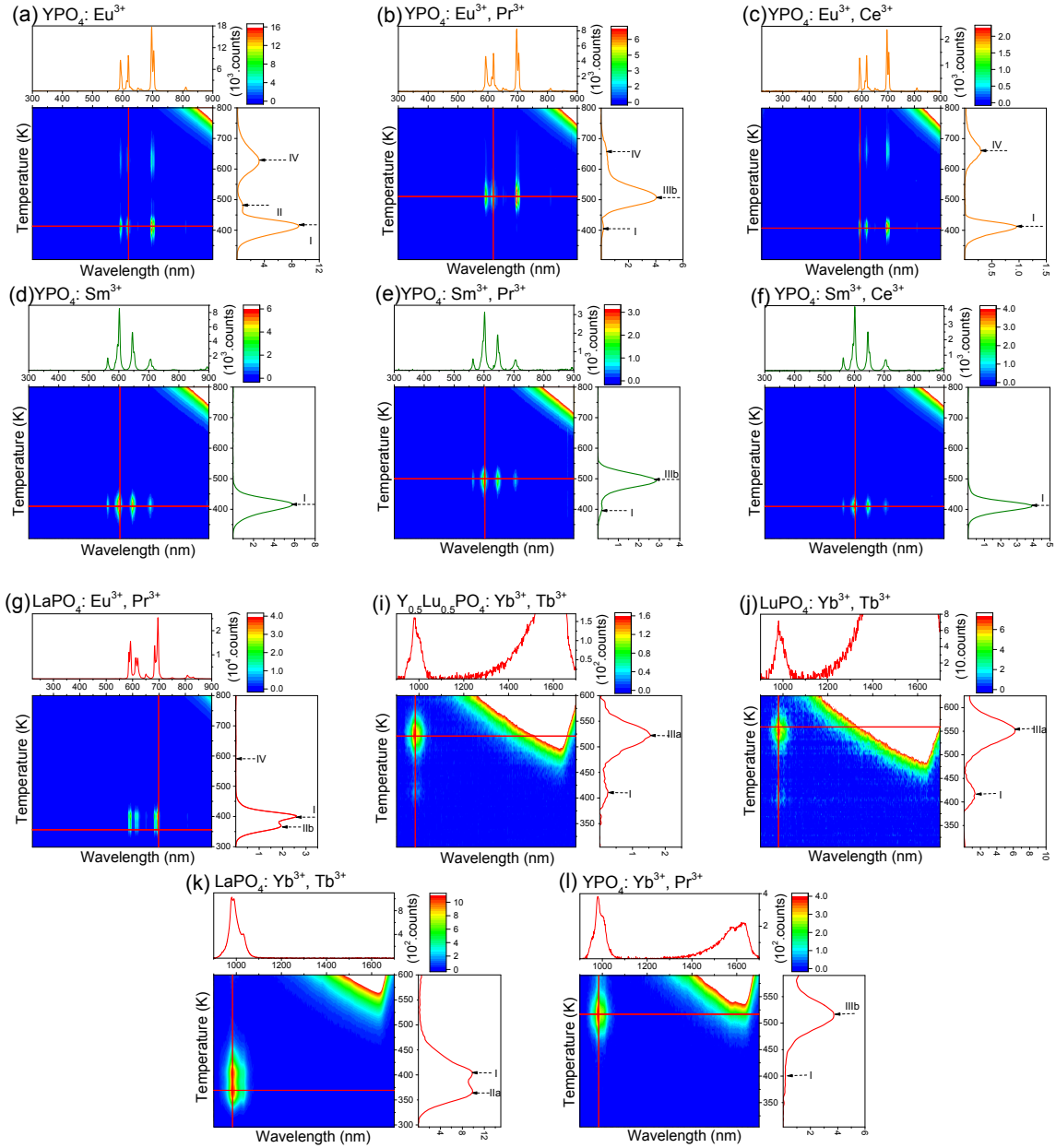


Fig. S4. Thermoluminescence emission (TLEM) plots of $\text{REPO}_4:0.005\text{Ln}^{3+}$ (RE=La, Y, and Lu) samples recorded at the heating rate of 1 K/s.

Compared to $\text{YPO}_4:0.005\text{Yb}^{3+},0.005\text{Tb}^{3+}$ (Fig. 8c), it is also noticed in Fig. S4i-j that the glow peak IIIa from the Tb^{3+} hole tapping center shifts about 45 K (0.33 eV) towards higher temperature in the $\text{Y}_{1-x}\text{Lu}_x\text{PO}_4:0.005\text{Yb}^{3+},0.005\text{Tb}^{3+}$ solid solutions with increasing x leading to the decreasing of the VRBE at the valence band top and the increased hole trap depth of Tb^{3+} . This observation is similar to that of glow peaks IIIa and IIIb shifting in $\text{Y}_{1-x}\text{Lu}_x\text{PO}_4:0.005\text{Eu}^{3+},0.005\text{Tb}^{3+}$ (Fig. 10) and $\text{Y}_{1-x}\text{Lu}_x\text{PO}_4:0.005\text{Eu}^{3+},0.005\text{Pr}^{3+}$ solid solutions (Fig. S7).

Note that the glow at around 1200-1700 nm appears in Fig. Si-l, which is due to blackbody radiation.

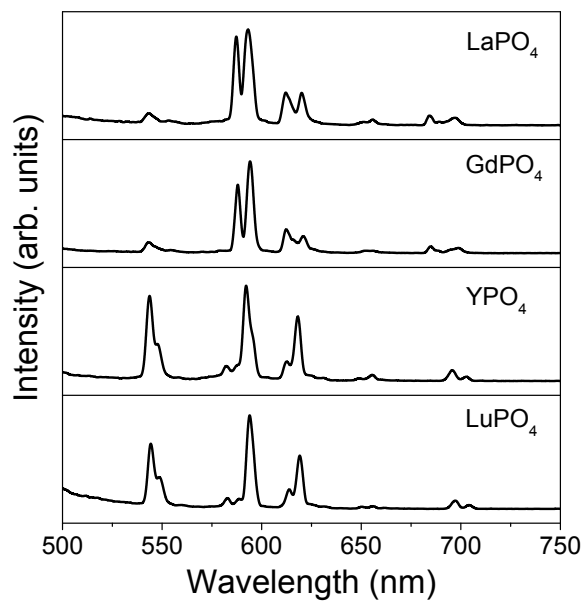


Fig. S5. Photoluminescence spectra of REPO₄:0.005Eu³⁺,0.005Tb³⁺ (RE=La, Gd, Y, and Lu) at 10 K. Samples were excited at the Eu³⁺-CT peak maxima.

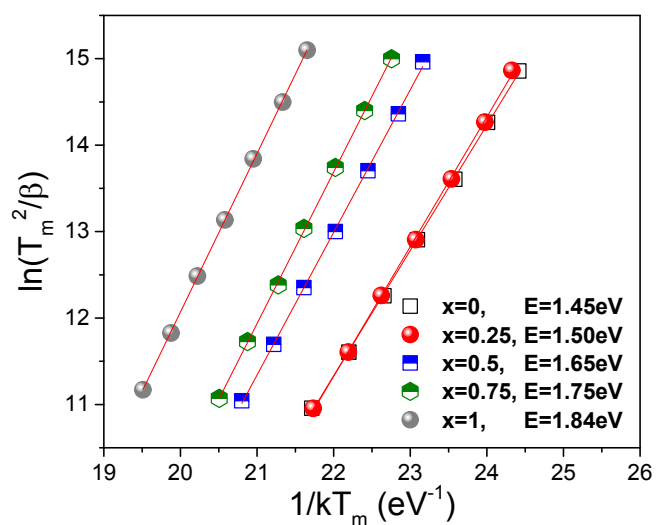


Fig. S6. Variable heating rate plots of Y_{1-x}Lu_xPO₄:0.005Eu³⁺,0.005Tb³⁺ solid solutions. The used heating rates were 0.08, 0.15, 0.30, 0.63, 1.25, 2.5, and 5 K/s.

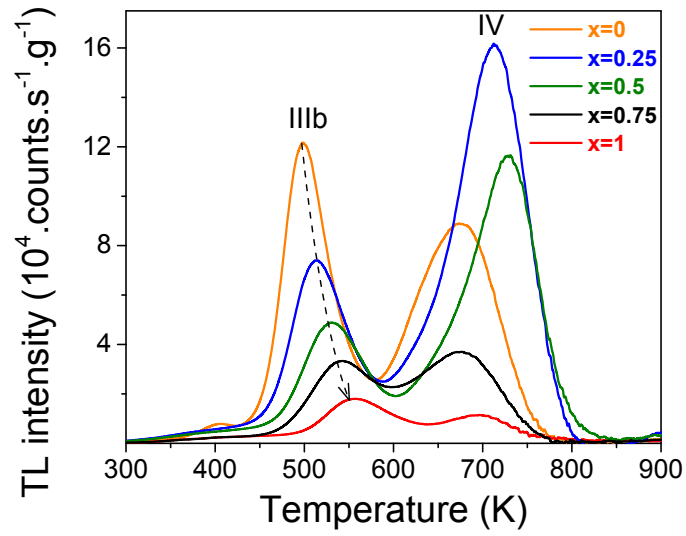


Fig. S7. TL glow curves for $Y_{1-x}Lu_xPO_4:0.005Eu^{3+},0.005Pr^{3+}$ solid solutions monitoring the emission from Eu^{3+} at the heating rate of 1 K/s.

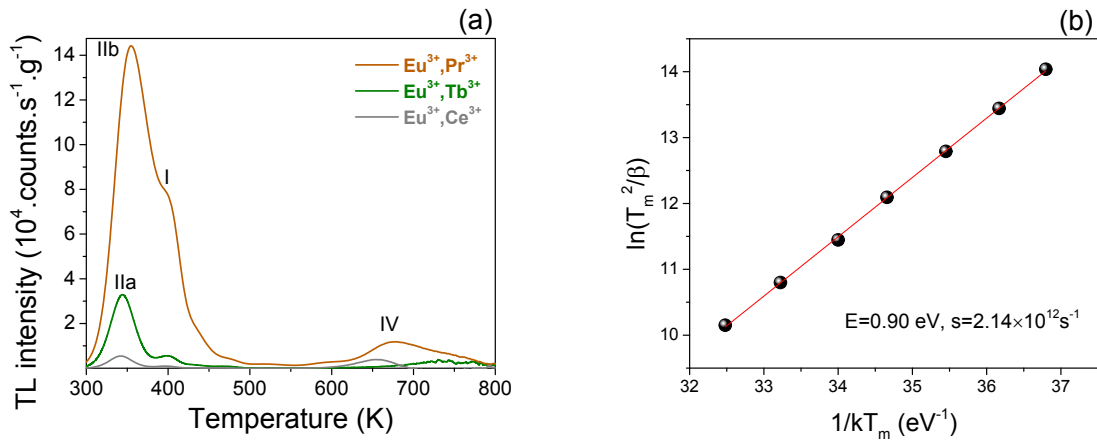


Fig. S8. (a) TL glow curves for $LaPO_4:0.005Eu^{3+},0.005Ln^{3+}$ ($Ln=Tb, Pr, \text{ and } Ce$) monitoring the Eu^{3+} emission at 300-800 K at the heating rate of 1 K/s. (b) variable heating rate plot of $LaPO_4:0.005Eu^{3+},0.005Tb^{3+}$ sample. The used heating rates are 0.08, 0.15, 0.30, 0.63, 1.25, 2.5, and 5 K/s.

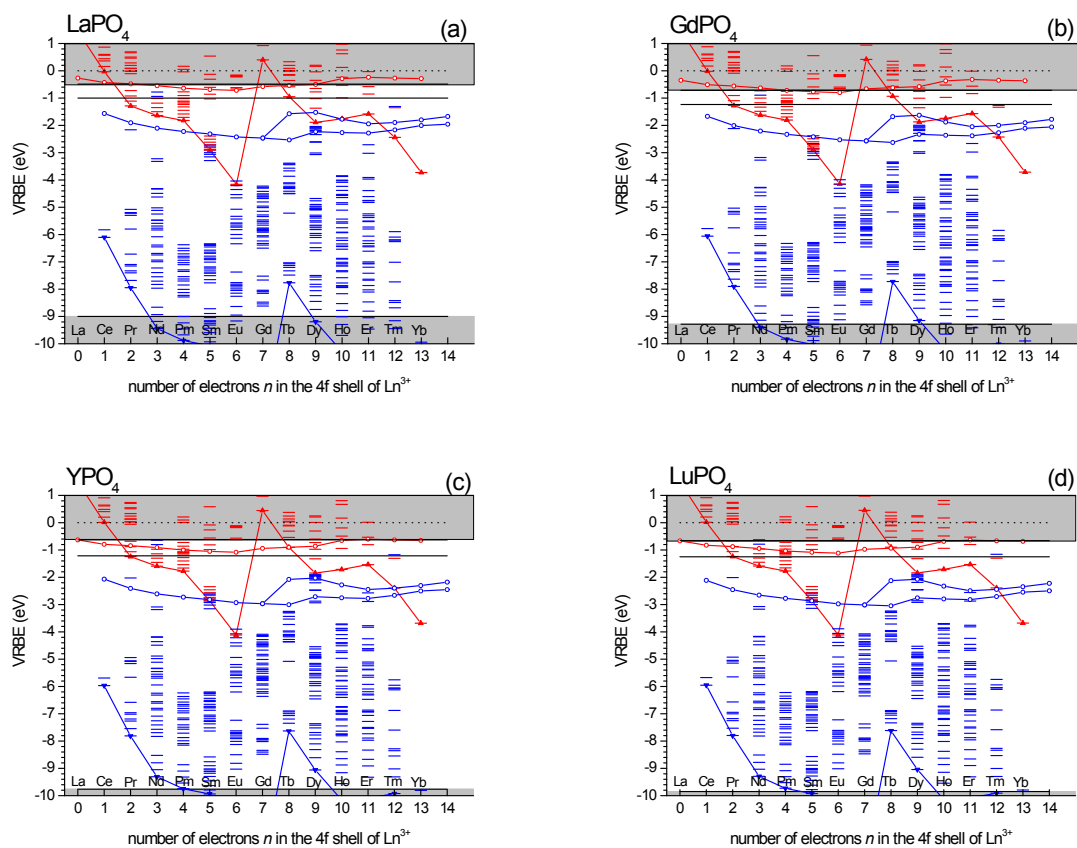


Fig. S9. Vacuum referred binding energy (VRBE) diagrams of all lanthanide levels in (a) LaPO_4 , (b) GdPO_4 , (c) YPO_4 , and (d) LuPO_4 .

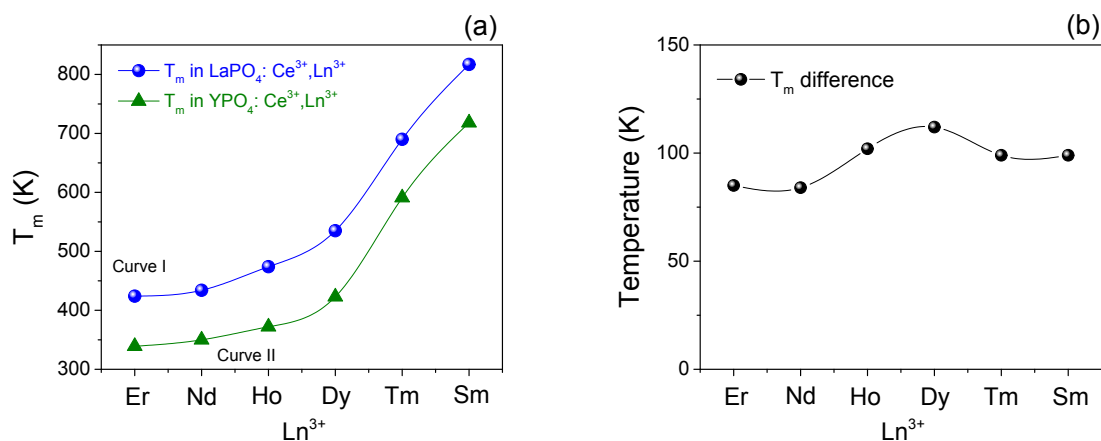


Fig. S10. (a) Peaks T_m for the TL glow curves of $REPO_4:0.005Ce^{3+},0.005Ln^{3+}$ (RE=La and Y) and (b) T_m difference between curve I and curve II.

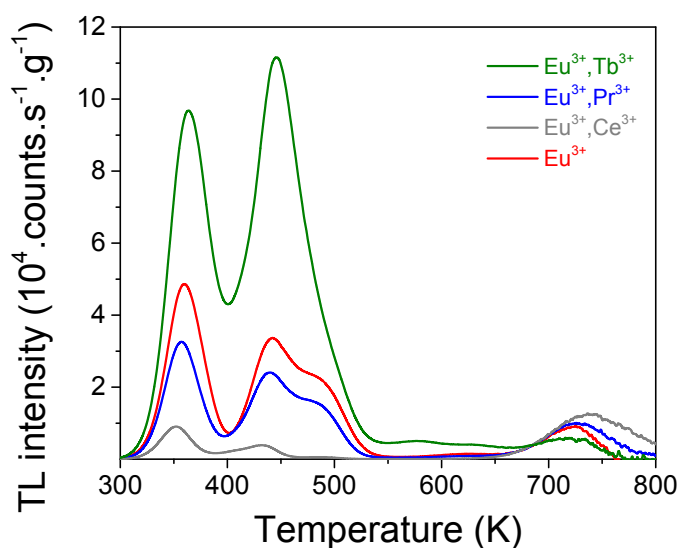


Fig. S11. TL glow curves for $GdPO_4:0.005Eu^{3+},0.005Ln^{3+}$ (Ln=Tb, Pr, and Ce) samples monitoring the Eu^{3+} emission at the heating rate of 1 K/s.

Reference

1. K. Van den Eeckhout, A. J. J. Bos, D. Poelman and P. F. Smet, *Physical Review B*, 2013, **87**, 045126.
2. J. Nahum and A. Halperin, *Journal of Physics and Chemistry of Solids*, 1963, **24**, 823-834.
3. K. H. Nicholas and J. Woods, *British Journal of Applied Physics*, 1964, **15**, 783.
4. G. F. J. Garlick and A. F. Gibson, *Proceedings of the Physical Society*, 1948, **60**, 574.
5. J. Ueda, P. Dorenbos, A. J. J. Bos, K. Kuroishi and S. Tanabe, *Journal of Materials Chemistry C*, 2015, **3**, 5642-5651.
6. Z. Wang, W. Wang, H. Zhou, J. Zhang, S. Peng, Z. Zhao and Y. Wang, *Inorganic Chemistry*, 2016, **55**, 12822-12831.